OPEN ACCESS Freely available online

PLOS ONE

On Three-Dimensional Flow and Heat Transfer over a Non-Linearly Stretching Sheet: Analytical and Numerical Solutions

Junaid Ahmad Khan[1], Meraj Mustafa[2]*, Tasawar Hayat[3,4], Ahmed Alsaedi[4]

1 Research Centre for Modeling and Simulation (RCMS), National University of Sciences and Technology (NUST), Islamabad, Pakistan, **2** School of Natural Sciences (SNS), National University of Sciences and Technology (NUST), Islamabad, Pakistan, **3** Department of Mathematics, Quaid-I-Azam University, Islamabad, Pakistan, **4** Nonlinear Analysis and Applied Mathematics (NAAM) Research Group, King Abdulaziz University, Jeddah, Saudi Arabia

Abstract

This article studies the viscous flow and heat transfer over a plane horizontal surface stretched non-linearly in two lateral directions. Appropriate wall conditions characterizing the non-linear variation in the velocity and temperature of the sheet are employed for the first time. A new set of similarity variables is introduced to reduce the boundary layer equations into self-similar forms. The velocity and temperature distributions are determined by two methods, namely (i) optimal homotopy analysis method (OHAM) and (ii) fourth-fifth-order Runge-Kutta integration based shooting technique. The analytic and numerical solutions are compared and these are found in excellent agreement. Influences of embedded parameters on momentum and thermal boundary layers are sketched and discussed.

Citation: Khan JA, Mustafa M, Hayat T, Alsaedi A (2014) On Three-Dimensional Flow and Heat Transfer over a Non-Linearly Stretching Sheet: Analytical and Numerical Solutions. PLoS ONE 9(9): e107287. doi:10.1371/journal.pone.0107287

Editor: Zhonghao Rao, China University of Mining and Technology, China

Received July 23, 2014; **Accepted** August 13, 2014; **Published** September 8, 2014

Data Availability: The authors confirm that all data underlying the findings are fully available without restriction. All relevant data are within the paper.

Funding: The author(s) received no specific funding for this work.

Competing Interests: The authors have declared that no competing interests exist.

* Email: meraj_mm@hotmail.com

Introduction

The fundamental problem of two-dimensional flow due to stretching plane surface, initially discussed by Crane [1], is involved in various industrial processes such as metal and polymer extrusion, drawing of plastic films, paper production etc. Owing to such applications, the researchers have discussed this problem under various aspects including suction or injection, variable surface temperature, convective boundary condition, mass transfer, mixed convection etc. The three-dimensional flow due to plane bi-directional linearly stretching sheet was first discussed by Wang [2]. He found an exact similarity solution of the classical Navier-Stokes equations. Later, Lakshmisha et al. [3] numerically examined the unsteady three-dimensional flow with heat and mass transfer over an unsteady stretching sheet. In contrast to this problem, Takhar et al. [4] investigated the three-dimensional flow of an electrically conducting fluid due to an impulsive motion of the stretching sheet. Ariel [4] derived approximate analytic and numeric solutions for steady three-dimensional flow over a stretching sheet. Xu et al. [5] provided uniformly valid series solutions for three-dimensional unsteady flow caused by the impulsively stretching sheet. Liu and Andersson [6] considered the heat transfer in three-dimensional flow due to non-isothermal stretching sheet. The unsteady three-dimensional flow of elastico-viscous fluid and mass transfer due to unsteady stretching sheet with constant wall concentration was studied by Hayat et al. [7]. In another paper, Hayat et al. [8] described the three-dimensional flow of Jeffrey fluid due to stretching sheet. Liu et al. [9] firstly discussed the three-dimensional flow due to exponentially stretching sheet numerically. Steady flow of nanofluid past a linearly bi-directional stretching sheet through Buongiorno's model was examined by Junaid et al. [10]. Sheikholeslami and Ganji [11] discussed the flow and heat transfer of nanofluid between parallel sheets in the presence of Brownian motion and thermophoresis effects.

The literature cited above deals only with the case of either linearly or exponentially driven velocity of the sheet. Vajravelu [12] numerically discussed the viscous flow due to stretching sheet when the velocity of the sheet was assumed to obey the power-law distribution, i.e. $u_w = cx^n$. He computed numerical solutions for various values of power-law index n. Cortell [13] extended this problem by considering viscous dissipation effects and variable surface temperature. The steady boundary layer flow of micro-polar fluid over non-linearly stretching sheet was discussed by Bhargava et al. [14]. Radiation and viscous dissipation effects on the boundary layer flow above a non-linearly stretching sheet were explored by Cortell [15]. Homotopy analytic solutions for mixed convection flow of micropolar fluid past a non-linearly stretching vertical sheet were obtained by Hayat et al. [16]. Kechil and Hashim [17] derived analytic solutions for MHD flow over a non-linearly stretching sheet by Adomian decomposition method. Hayat et al. [18] used modified decomposition method for the series solutions of MHD flow of an electrically conducting fluid over a non-linearly stretching surface. The impact of chemical reaction on the flow over a non-linearly stretching sheet embedded in a porous medium was investigated by Ziabakhsh et al. [19]. Rana and Bhargava [20] computed numerical solutions for two-dimensional flow of nanofluid due to non-linearly stretching sheet

by finite element method. Shahzad et al. [21] obtained closed form exact solutions for axisymmetric flow and heat transfer when the velocity of the stretching sheet was proportional to r^3. Partial slip effects on the boundary layer flow past a non-linearly permeable stretching surface have been addressed by Mukhopadhyay [22]. In another paper, Mukhopadhyay [23] analyzed the flow and heat transfer of Casson fluid due to non-linearly stretching sheet. Rashidi et al. [24] derived homotopy based analytic solutions for flow over a non-isothermal stretching plate with transpiration.

To our knowledge, the three-dimensional flow due to non-linearly stretching sheet has not been yet reported. It is obvious that three-dimensional flows can be appropriate in giving more clear physical insights of the real world problem when compared with the two-dimensional flows. The present work is therefore undertaken to fill such a void. The study also assumes that the temperature across the sheet is non-linearly distributed. Introducing a new set of similarity variables the boundary layer equations are first reduced into self-similar forms and then solved both analytically and numerically. It is pertinent to mention that computation of either approximate analytic or numerical solutions of the boundary layer equations governing the flow and heat transfer is often challenging (see [25–33] for details). Attention is focused on the physical interpretation of parameters including the power-law index n.

Mathematical Modeling

Let us consider the three-dimensionalincompressible flow over a plane elastic sheet located at $z=0$ as shown in the Fig. 1. The flow is induced due to stretching of the sheet in two lateral directions. Let $U_w(x,y)=a(x+y)^n$ and $V_w(x,y)=b(x+y)^n$ be the velocities of the sheet along the $x-$ and $y-$ directions respectively with $a,b,n>0$ are constants (see Table 1). $T_w(x,y)=T_\infty+A(x+y)^n$ is the variable surface temperature where $A>0$ is constant and T_∞ is the ambient fluid temperature. Under the usual boundary layer assumptions, the equations governing the three-dimensional flow and heat transfer in the absence of viscous dissipation and internal heat generation/absorption can be expressed as (see Liu et al. [9])

$$\frac{\partial u}{\partial x}+\frac{\partial v}{\partial y}+\frac{\partial w}{\partial z}=0, \tag{1}$$

$$u\frac{\partial u}{\partial x}+v\frac{\partial u}{\partial y}+w\frac{\partial u}{\partial z}=\nu\frac{\partial^2 u}{\partial z^2}, \tag{2}$$

$$u\frac{\partial v}{\partial x}+v\frac{\partial v}{\partial y}+w\frac{\partial v}{\partial z}=\nu\frac{\partial^2 v}{\partial z^2}, \tag{3}$$

$$u\frac{\partial T}{\partial x}+v\frac{\partial T}{\partial y}+w\frac{\partial T}{\partial z}=\alpha\frac{\partial^2 T}{\partial z^2}, \tag{4}$$

where u,v and w are the velocity components along the x,y and $z-$ directions respectively, ν is the kinematic viscosity, T is the fluid temperature and α is the thermal diffusivity (see Table 1). The boundary conditions are imposed as under:

$$\begin{aligned} &u=U_w=a(x+y)^n, v=V_w=b(x+y)^n, w=0,\\ &T=T_w=T_\infty+A(x+y)^n \text{ at } z=0,\\ &u=0, v=0, T\to T_\infty \text{ as } z\to\infty. \end{aligned} \tag{5}$$

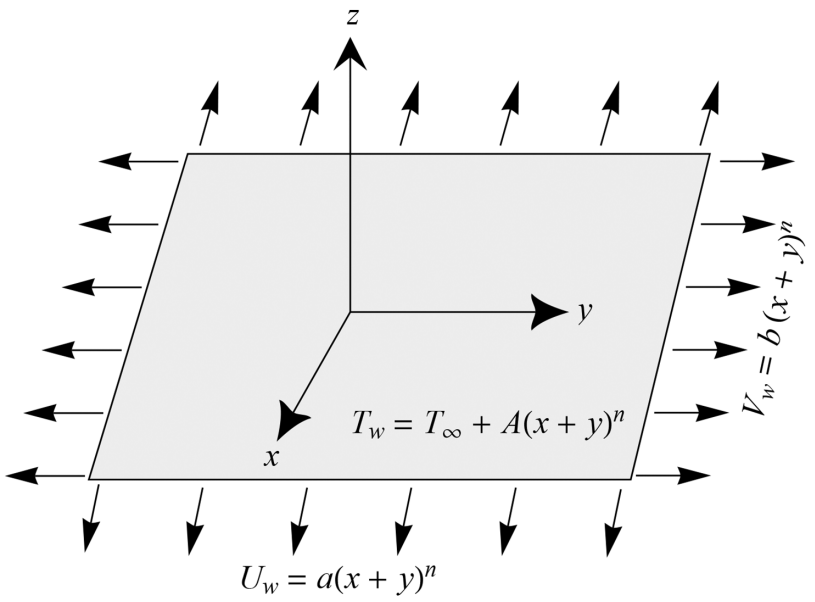

Figure 1. Physical configuration and coordinate system.
doi:10.1371/journal.pone.0107287.g001

Table 1. List of symbols.

(x,y,z) **Cartesian coordinate system**	k **thermal conductivity**
u,v,w velocity components along the $x-,y-,z-$ directions	$\hbar$ non-zero auxiliary parameter
U_w,V_w velocity of the stretching sheet along $x-$ and $y-$ direction	$'$ 1st order derivative with respect to η
T fluid temperature	$''$ 2nd order derivative with respect to η
T_w wall temperature	$'''$ 3rd order derivative with respect to η
T_∞ ambient fluid temperature	***Greek symbols***
a,b,A positive constants	ν kinematic viscosity
n Power-law index	α thermal diffusivity
f,g dimensionless stream function	θ dimensionless temperature
Pr Prandtl number	η similarity variable
C_{fx},C_{fy} skin friction coefficient along $x-$ and $y-$ direction	λ ratio of the stretching rates
Nu local Nusselt number	τ_{zx},τ_{zy} wall shear stress along $x-$ and $y-$ direction
q_w wall heat flux	ρ density of the fluid
$\mathrm{Re}_x,\mathrm{Re}_y$ local Reynolds number along $x-$ and $y-$ direction	μ dynamic viscosity

doi:10.1371/journal.pone.0107287.t001

We introduce the new similarity transformations as follows:

$$\begin{aligned} u&=a(x+y)^n f'(\eta),\ v=a(x+y)^n g'(\eta),\ w\\ &=-\sqrt{av}(x+y)^{\frac{n-1}{2}}\left(\frac{n+1}{2}(f+g)+\frac{n-1}{2}\eta(f'+g')\right),\\ \theta(\eta)&=\frac{T-T_\infty}{T_w-T_\infty},\quad \eta=\sqrt{\frac{a}{\nu}}(x+y)^{\frac{n-1}{2}}z. \end{aligned} \tag{6}$$

We have modified the similarity transformations used by Liu et al. [9] for the current problem. Using (6), Eq.(1) is identically satisfied and Eqs. (2)–(5) become

$$f'''+\frac{n+1}{2}(f+g)f''-n(f'+g')f'=0, \tag{7}$$

$$g'''+\frac{n+1}{2}(f+g)g''-n(f'+g')g'=0, \tag{8}$$

$$\frac{1}{Pr}\theta''+\frac{n+1}{2}(f+g)\theta'-n(f'+g')\theta=0, \tag{9}$$

$$f(0)=g(0)=0, f'(0)=1,\ g'(0)=\lambda,\ \theta(0)=1, \tag{10}$$

$$f'(\infty)\to 0, g'(\infty)\to 0, \theta(\infty)\to 0,$$

where $Pr=\nu/\alpha$ is the Prandtl number and $\lambda=b/a$ is the ratio of stretching rate along the $y-$ direction to the stretching rate along the $x-$ direction (see Table 1). The above equations reduce to the case of two-dimensional flow when $\lambda=0$. Moreover, when $\lambda=1$, the equations governing the axisymmetric flow due to non-linearly stretching sheet are recovered. When $\mathrm{Pr}=1$ the solution of f' is also a solution of θ. The quantities of practical interest are the skin friction coefficients and the local Nusselt number which are defined as below:

$$C_{fx}=\frac{\tau_{zx}}{\rho U_w^2}, C_{fy}=\frac{\tau_{zy}}{\rho V_w^2},\ Nu=\frac{(x+y)q_w}{k(T_w-T_\infty)}, \tag{11}$$

where τ_{zx} and τ_{zy} are the wall shear stresses and q_w is the wall heat flux. These are given by

$$\begin{aligned} \tau_{zx}=\mu\left(\frac{\partial u}{\partial z}+\frac{\partial w}{\partial x}\right)_{z=0}, \tau_{zy}=\mu\left(\frac{\partial v}{\partial z}+\frac{\partial w}{\partial y}\right)_{z=0},\\ q_w=-k\left(\frac{\partial T}{\partial z}\right)_{z=0}, \end{aligned} \tag{12}$$

using Eqs. (6) and (12) in Eq. (11), one obtains

$$\begin{aligned} \mathrm{Re}_x^{1/2}C_{fx}&=f''(0),\\ \mathrm{Re}_y^{1/2}\lambda^{3/2}C_{fy}&=g''(0),\\ \mathrm{Re}_x^{-1/2}Nu&=-\theta'(0), \end{aligned} \tag{13}$$

where $\mathrm{Re}_x=U_w(x+y)/\nu$ and $\mathrm{Re}_y=V_w(x+y)/\nu$ are the local Reynolds numbers along the $x-$ and $y-$ directions respectively (see Table 1). The vertical component of velocity at the far field boundary can be expressed as

$$w(x,y,\infty)=-\sqrt{av(x+y)^{n-1}}\,\frac{n+1}{2}[f(\infty)+g(\infty)]. \tag{14}$$

Optimal homotopy analytic solutions

The non-linear differential equations (7)–(9) with the boundary conditions (10) have been solved by optimal homotopy analysis

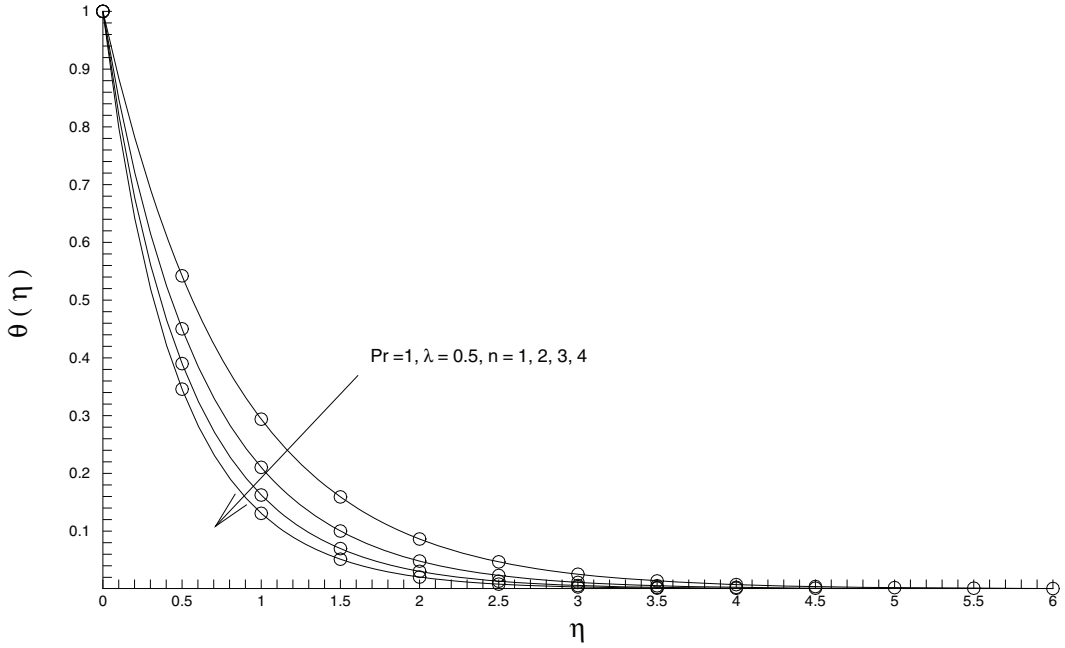

Figure 2. Comparison of analytical and numerical solutions for the temperature distribution. Lines: 15th-order OHAM solutions, Circles: Numerical solution.
doi:10.1371/journal.pone.0107287.g002

method (OHAM) [34,35]. For this purpose, we first select the initial guesses f_0, g_0 and θ_0 of $f(\eta)$, $g(\eta)$ and $\theta(\eta)$ as under:

$$f_0(\eta)=1-\exp(-\eta),\quad g_0(\eta)=\lambda[1-\exp(-\eta)],\quad \theta_0(\eta)=\exp(-\eta), \tag{15}$$

and the auxiliary linear operators are selected as below

$$\boldsymbol{L}_f(f)=\frac{d^3f}{d\eta^3}-\frac{df}{d\eta},\quad \boldsymbol{L}_g(g)=\frac{d^3g}{d\eta^3}-\frac{dg}{d\eta},\quad \boldsymbol{L}_\theta(\theta)=\frac{d^2\theta}{d\eta^2}-\theta. \tag{16}$$

If $q\in[0,1]$ is the embedding parameter and $\hbar$ the non-zero auxiliary parameter, then the generalized homotopic equations

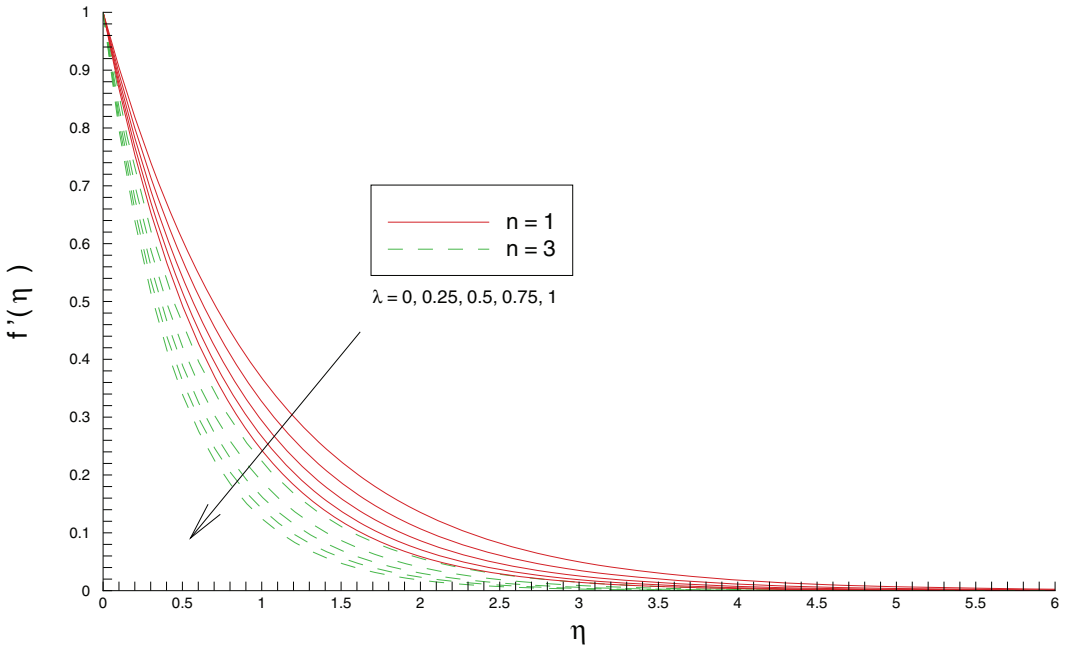

Figure 3. Influence of stretching rates ratio λ on the $x-$ component of velocity f'.
doi:10.1371/journal.pone.0107287.g003

corresponding to (7)–(10) can be written as follows

$$(1-q)\boldsymbol{L}_f[F(\eta;\,q)-f_0(\eta)]=q\hbar\boldsymbol{N}_f[F(\eta;\,q),G(\eta;\,q)], \quad (17)$$

$$(1-q)\boldsymbol{L}_g[G(\eta;\,q)-g_0(\eta)]=q\hbar\boldsymbol{N}_g[F(\eta;\,q),G(\eta;\,q)], \quad (18)$$

$$(1-q)\boldsymbol{L}_\theta[\Theta(\eta;\,q)-\theta_0(\eta)]=q\hbar\boldsymbol{N}_\theta[F(\eta;\,q),G(\eta;\,q),\Theta(\eta;\,q)], \quad (19)$$

$$\begin{aligned} &F(\eta;\,q)|_{\eta=0}=0,\frac{\partial F(\eta;\,q)}{\partial\eta}\bigg|_{\eta=0}=1,\\ &G(\eta;\,q)|_{\eta=0}=0,\frac{\partial G(\eta;\,q)}{\partial\eta}\bigg|_{\eta=0}=\lambda,\ \Theta(\eta;\,q)|_{\eta=0}=0,\\ &\frac{\partial F(\eta;\,q)}{\partial\eta}\bigg|_{\eta\to\infty}=0,\ \frac{\partial G(\eta;\,q)}{\partial\eta}\bigg|_{\eta\to\infty}=0,\ \Theta(\eta;\,q)\bigg|_{\eta\to\infty}=0, \end{aligned} \quad (20)$$

where the non-linear operators $\boldsymbol{N}_f$, $\boldsymbol{N}_g$ and $\boldsymbol{N}_\theta$ are

$$\begin{aligned} &\boldsymbol{N}_f[F(\eta;\,q),G(\eta;\,q)]\\ &=\frac{\partial^3F(\eta;\,q)}{\partial\eta^3}+\frac{n+1}{2}(F(\eta;\,q)+G(\eta;\,q))\frac{\partial^2F(\eta;\,q)}{\partial\eta^2}\\ &-n\left(\frac{\partial F(\eta;\,q)}{\partial\eta}+\frac{\partial G(\eta;\,q)}{\partial\eta}\right)\frac{\partial F(\eta;\,q)}{\partial\eta}, \end{aligned} \quad (21)$$

$$\begin{aligned} &\boldsymbol{N}_g[F(\eta;\,q),G(\eta;\,q)]\\ &=\frac{\partial^3G(\eta;\,q)}{\partial\eta^3}+\frac{n+1}{2}(F(\eta;\,q)+G(\eta;\,q))\frac{\partial^2G(\eta;\,q)}{\partial\eta^2}\\ &-n\left(\frac{\partial F(\eta;\,q)}{\partial\eta}+\frac{\partial G(\eta;\,q)}{\partial\eta}\right)\frac{\partial G(\eta;\,q)}{\partial\eta}, \end{aligned} \quad (22)$$

$$\begin{aligned} &\boldsymbol{N}_\theta[F(\eta;q),G(\eta;\,q),\Theta(\eta;q)]\\ &=\frac{1}{\mathrm{Pr}}\frac{\partial^2\Theta(\eta;\,q)}{\partial\eta^2}+\left(\frac{n+1}{2}\right)(F(\eta;p)+G(\eta;q))\frac{\partial\Theta(\eta;\,q)}{\partial\eta}\\ &-n\left(\frac{\partial F(\eta;\,q)}{\partial\eta}+\frac{\partial G(\eta;\,q)}{\partial\eta}\right)\Theta(\eta;\,q). \end{aligned} \quad (23)$$

By Taylor's series expansion one obtains

$$F(\eta;\,q)=f_0(\eta)+\sum_{m=1}^{\infty}f_m(\eta)q^m;f_m(\eta)=\frac{1}{m!}\frac{\partial^mF(\eta;\,q)}{\partial q^m}\bigg|_{q=0}, \quad (24)$$

$$G(\eta;\,q)=g_0(\eta)+\sum_{m=1}^{\infty}g_m(\eta)q^m;g_m(\eta)=\frac{1}{m!}\frac{\partial^mG(\eta;\,q)}{\partial q^m}\bigg|_{q=0}, \quad (25)$$

$$\Theta(\eta;\,q)=\theta_0(\eta)+\sum_{m=1}^{\infty}\theta_m(\eta)q^m;\theta_m(\eta)=\frac{1}{m!}\frac{\partial^m\Theta(\eta;\,q)}{\partial q^m}\bigg|_{q=0}. \quad (26)$$

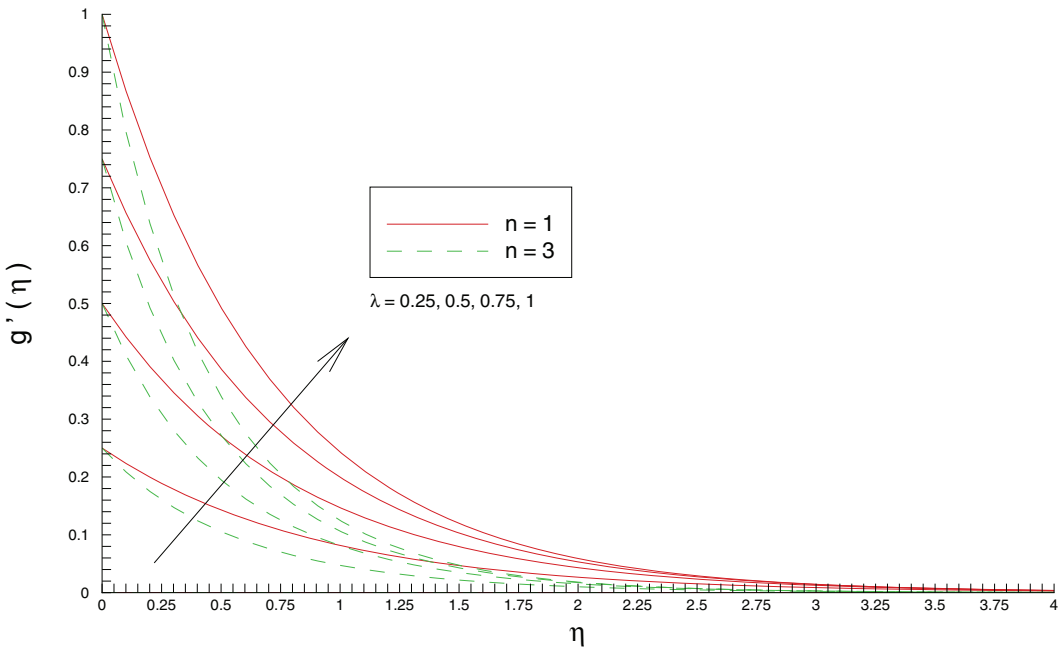

Figure 4. Influence of stretching rates ratio λ on the $y-$ component of velocity g'.
doi:10.1371/journal.pone.0107287.g004

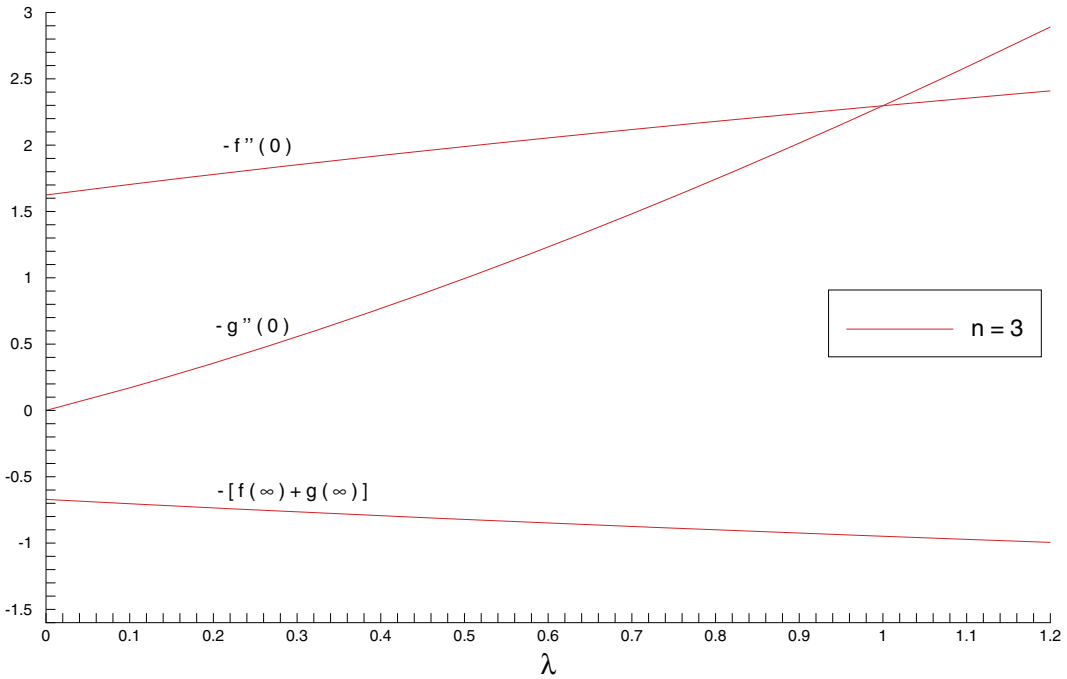

Figure 5. Influence of stretching rates ratio λ on the skin friction coefficients $f''(0)$ and $g''(0)$ and entrainment velocity $f(\infty)+g(\infty)$.
doi:10.1371/journal.pone.0107287.g005

Substituting $q=1$ in the above equations yields the final result. The functions f_m, g_m and θ_m can be determined from the deformation of Eqs. (7)–(10). Explicitly the mth-order deformation equations corresponding to Eqs. (7)–(10) are as below

$$\boldsymbol{L}_f[f_m(\eta)-\chi_m f_{m-1}(\eta)]=\hbar \boldsymbol{R}_m^f(\eta), \tag{27}$$

$$\boldsymbol{L}_g[g_m(\eta)-\chi_m g_{m-1}(\eta)]=\hbar \boldsymbol{R}_m^g(\eta), \tag{28}$$

$$\boldsymbol{L}_\theta[\theta_m(\eta)-\chi_m \theta_{m-1}(\eta)]=\hbar \boldsymbol{R}_m^\theta(\eta), \tag{29}$$

$$\begin{aligned} &f_m(0)=0,\ \left.\frac{df_m(\eta)}{d\eta}\right|_{\eta=0}=0,\\ &\mathrm{g}_m(0)=0,\ \left.\frac{dg_m(\eta)}{d\eta}\right|_{\eta=0}=0,\ \theta_m(0)=0,\\ &\left.\frac{\partial f_m(\eta)}{\partial \eta}\right|_{\eta\to+\infty}=0,\ \left.\frac{\partial g_m(\eta)}{\partial \eta}\right|_{\eta\to+\infty}=0,\ \theta_m(\infty)=0, \end{aligned} \tag{30}$$

$$\begin{aligned} \boldsymbol{R}_m^f(\eta)=&\frac{d^3 f_{m-1}}{d\eta^3}+\sum_{k=0}^{m-1}\left[\frac{n+1}{2}(f_{m-1-k}+g_{m-1-k})\frac{d^2 f_k}{d\eta^2}-\right.\\ &\left. n\left(\frac{df_{m-1-k}}{d\eta}+\frac{dg_{m-1-k}}{d\eta}\right)\frac{df_k}{d\eta}\right], \end{aligned} \tag{31}$$

$$\begin{aligned} \boldsymbol{R}_m^g(\eta)=&\frac{d^3 g_{m-1}}{d\eta^3}+\sum_{k=0}^{m-1}\left[\frac{n+1}{2}(f_{m-1-k}+g_{m-1-k})\frac{d^2 g_k}{d\eta^2}-\right.\\ &\left. n\left(\frac{df_{m-1-k}}{d\eta}+\frac{dg_{m-1-k}}{d\eta}\right)\frac{dg_k}{d\eta}\right], \end{aligned} \tag{32}$$

$$\begin{aligned} \boldsymbol{R}_m^\theta(\eta)=&\frac{1}{\mathrm{Pr}}\frac{d^2\theta_{m-1}}{d\eta^2}+\sum_{k=0}^{m-1}\left[\frac{n+1}{2}(f_{m-1-k}+g_{m-1-k})\frac{d\theta_k}{d\eta}-\right.\\ &\left. n\left(\frac{df_{m-1-k}}{d\eta}+\frac{dg_{m-1-k}}{d\eta}\right)\theta_k\right], \end{aligned} \tag{33}$$

$$\chi_m=\begin{cases} 0, m\le 1,\\ 1, m>1. \end{cases} \tag{34}$$

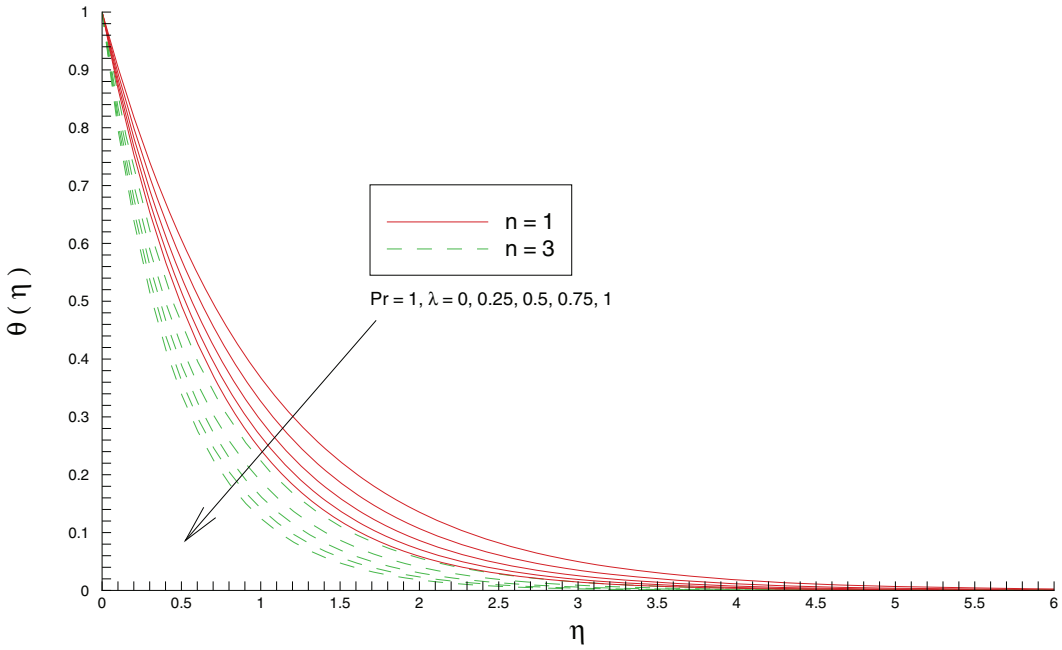

Figure 6. Influence of stretching rates ratio λ on the temperature θ.
doi:10.1371/journal.pone.0107287.g006

In order to determine the optimal values of $\hbar$ we define the squared residuals of the governing Eqs. (7)–(10), ζ_M^f, ζ_M^g and ζ_M^θ as

$$\zeta_M^f = \int_0^\infty \left[N_f \left(\sum_{j=0}^{M} f_j(\eta), \sum_{j=0}^{M} g_j(\eta) \right) \right]^2 \mathrm{d}\eta, \tag{35}$$

$$\zeta_M^g = \int_0^\infty \left[N_g \left(\sum_{j=0}^{M} f_j(\eta), \sum_{j=0}^{M} g_j(\eta) \right) \right]^2 \mathrm{d}\eta, \tag{36}$$

$$\zeta_M^\theta = \int_0^\infty \left[N_\theta \left(\sum_{j=0}^{M} f_j(\eta), \sum_{j=0}^{M} g_j(\eta), \sum_{j=0}^{M} \theta_j(\eta) \right) \right]^2 \mathrm{d}\eta. \tag{37}$$

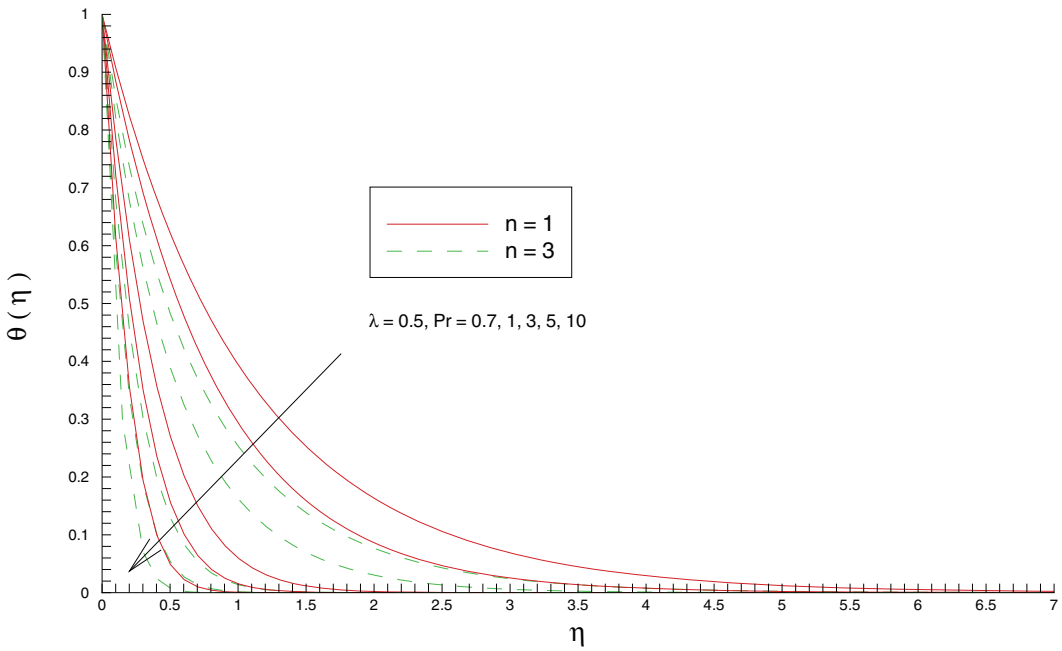

Figure 7. Influence of Prandtl number Pr on the temperature θ.
doi:10.1371/journal.pone.0107287.g007

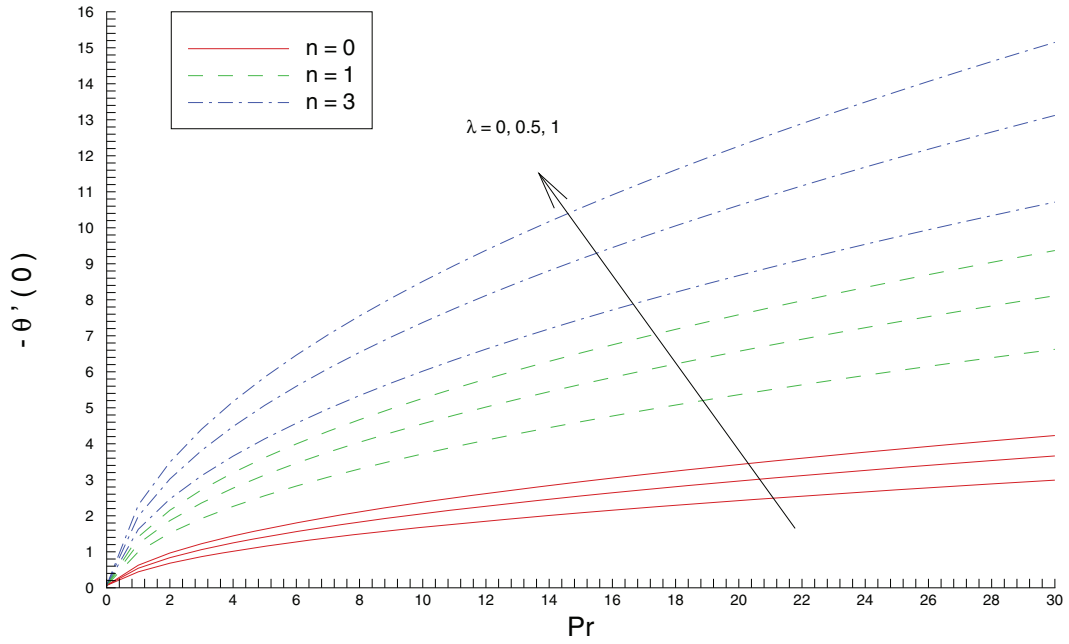

Figure 8. Influence of Prandtl number Pr **and stretching rates ratio** λ **on the wall temperature gradient** $\theta'(0)$.
doi:10.1371/journal.pone.0107287.g008

Such kind of error has been considered in other works [36–41]. The smaller $\zeta_M's$, the more accurate the mth order approximation of the solution. The optimal values of $\hbar$ can be obtained by minimizing the $\zeta_M's$, through the command *Minimize* of the software MATHEMATICA (see Liao [36] for details). Alternatively MATHEMATICA package bvph 2.0 can also be used to calculate such values (see [41] for details).

Numerical method

Eqs. (7)–(9) subject to the boundary conditions (10) have been solved numerically by shooting method with fifth order Runge-Kutta integration procedure. First, we reduce the original ODEs into a system of 1st order ODEs by substituting $x_1=f, x_2=f', x_3=f'', x_4=g, x_5=g', x_6=g'', x_7=\theta$ and $x_8=\theta'$ which gives

$$\begin{bmatrix} x_1' \\ x_2' \\ x_3' \\ x_4' \\ x_5' \\ x_6' \\ x_7' \\ x_8' \end{bmatrix} = \begin{bmatrix} x_2 \\ x_3 \\ -\frac{n+1}{2}(x_1+x_4)x_3+n(x_2+x_5)x_2 \\ x_5 \\ x_6 \\ -\frac{n+1}{2}(x_1+x_4)x_6+n(x_2+x_5)x_5 \\ x_8 \\ -\Pr\left(\frac{n+1}{2}(x_1+x_4)x_8-n(x_2+x_5)x_7\right) \end{bmatrix}, \quad (38)$$

Table 2. Numerical values of $f''(0)$ and $g''(0)$ for different values of n and λ.

n	λ	$f''(0)$		$g''(0)$	
		shooting	bvp5c	shooting	bvp5c
1	0	−1	−1	0	0
	0.5	−1.224745	−1.224742	−0.612372	−0.612371
	1	−1.414214	−1.414214	−1.414214	−1.414214
3	0	−1.624356	−1.624356	0	0
	0.5	−1.989422	−1.989422	−0.994711	−0.994711
	1	−2.297186	−2.297182	−2.297186	−2.297182

doi:10.1371/journal.pone.0107287.t002

Table 3. Numerical values of local Nusselt number $-\theta'(0)$ for various values of n, Pr and λ.

n	Pr	λ	$-\theta'(0)$	
			shooting	bvp5c
1	0.7	0	0.793668	0.793668
		0.5	0.972033	0.972029
		1	1.122406	1.122321
	1	0	1.000000	0.999990
		0.5	1.224745	1.224742
		1	1.414214	1.414214
	7	0	3.072250	3.072251
		0.5	3.762723	3.762724
		1	4.344818	4.344779
3	0.7	0	1.292193	1.292194
		0.5	1.582607	1.582607
		1	1.827437	1.827427
	1	0	1.624356	1.624356
		0.5	1.989422	1.989422
		1	2.297186	2.297182
	7	0	4.968777	4.968777
		0.5	6.085484	6.085485
		1	7.026912	7.026913

doi:10.1371/journal.pone.0107287.t003

and the corresponding initial conditions are

$$\begin{bmatrix} x_1 \\ x_2 \\ x_3 \\ x_4 \\ x_5 \\ x_6 \\ x_7 \\ x_8 \end{bmatrix} = \begin{bmatrix} 0 \\ 1 \\ u_1 \\ 0 \\ \lambda \\ u_2 \\ 1 \\ u_3 \end{bmatrix}, \tag{39}$$

Suitable values of the unknown initial conditions $u_1 = f''(0), u_2 = g''(0)$ and $u_3 = \theta'(0)$ are guessed and then integration is carried out. The values of u_1, u_2 and u_3 are then iteratively computed through Newton's method such that the solutions satisfy the boundary conditions at infinity (given in Eq. (10)) with error less than 10^{-6}.

Results and Discussion

This section contains the physical interpretations of the behavior of the interesting parameters entering into the problem. We compare the 15^{th}-order OHAM solutions for temperature θ with the numerical ones for different values of n. Fig. 2 shows that data retrieved from both solution methods are identical, demonstrating the validation of our findings.

Figs. 3 and 4 show the variations in horizontal and vertical components of velocity with an increase in stretching rates ratio λ. It is clear that increase in λ corresponds to an increase in the stretching rate along the $y-$direction. Due to this reason the vertical component of velocity increases with an enhancement in λ while the velocity in the $x-$direction decreases correspondingly. The wall velocity gradients $f''(0), g''(0)$ and entrainment velocity $f(\infty)+g(\infty)$ as functions of stretching rates ratio λ have been plotted in Fig. 5. Due to the bi-directional stretching sheet, there will be downward flow in the vertical direction. The vertical component at far field boundary is therefore expected to be negative in this situation. We notice that shear stresses at the wall increase when λ is increased. Further, the larger values of λ enhances the velocity of the cold fluid at the ambient. As a consequence, the entrainment velocity is an increasing function of λ.

Fig. 6 indicates that temperature θ decreases with an increase in stretching rates ratio λ for unity Prandtl number. Physically, an increase in λ enhances the intensity of colder fluid at the ambient (as noticed in Fig. 6) towards the hot sheet which eventually corresponds to decrease the local fluid temperature. Fig. 7 perceives the behavior of Prandtl number Pr on the temperature. A bigger Prandtl number fluid has less thermal diffusivity and hence it allows less thermal effect to penetrate deeper into the fluid. As a result, temperature decreases and the thermal boundary layer becomes thinner when Pr is increased. This decrease in thickness of the thermal boundary layer is compensated with a larger wall slope of temperature function.

Fig. 8 plots the wall temperature gradient against Pr with the variation in stretching rates ratio λ. The wall heat transfer rate approaches the zero value for vanishing Prandtl number $\text{Pr} \to 0$, a fact that is clear from the energy equation (9). Moreover, this Fig. compliments the results of Fig. 4. In bigger Prandtl number fluids the convection is effective in transferring energy from the stretching sheet compared to pure conduction. Due to this reason the wall heat transfer rate is an increasing function of Pr. The reduction in thermal boundary layer thickness with an increase in λ meets with the bigger magnitude of local Nusselt number. In other words the enhanced intensity of cold fluid at the ambient

towards the hot fluid closer to the sheet results in larger heat transfer rate at the sheet.

Tables 2 and 3 provide the numerical values of skin friction coefficients and local Nusselt number for different values of parameters by employing shooting method. The results are compared with the MATLAB built in function bvp5c and found in excellent agreement. We notice that wall shear stresses increase with an increase in λ more rapidly at $n=3$ when compared with $n=1$. The thinner thermal boundary layer accounted for larger n accompanies with larger temperature gradient along the sheet. The magnitude of increase in wall temperature gradient $\theta'(0)$ with an increase in Pr increases when n is increased.

Conclusions

For the first time, the flow and heat transfer over a plane surface stretched non-linearly in two lateral directions have been investigated. The simulation in this study assumes that the temperature across the sheet is non-linearly distributed. Both analytic and numerical solutions are obtained and found in excellent agreement. Following are the major results of this study.

I. It is seen that shear stress at the wall increase when the stretching rates ratio is increased. The entrainment velocity is negative, representing a downward flow in the vertical direction, which is a consequence of the bi-directional stretching sheet.

II. The increased intensity of the cold fluid at the ambient towards the stretching sheet with an increase in stretching rates ratio λ decreases the fluid temperature.

III. The temperature decreases and thermal boundary layer thins when the power-law index n is increased.

IV. The results for the case of two-dimensional and axisymmetric flows can be obtained as special cases of present study when $\lambda=0$ and $\lambda=1$ respectively.

Author Contributions

Analyzed the data: JAK MM TH AA. Contributed reagents/materials/analysis tools: JAK MM TH AA. Contributed to the writing of the manuscript: JAK MM TH.

References

1. Crane LJ (1970). Flow past a stretching plate. Z Angew Math Phys, 21(4), 645–647.
2. Wang CY (1984). The three-dimensional flow due to a stretching flat surface. Phys Fluids, 27(8), 1915–1917.
3. Lakshmisha KN, Venkateswaran S, Nath G (1988). Three-dimensional unsteady flow with heat and mass transfer over a continuous stretching surface. J Heat Trans, 110(3), 590–595.
4. Takhar HS, Chamkha AJ, Nath G (2001). Unsteady three-dimensional MHD-boundary-layer flow due to the impulsive motion of a stretching surface. Acta Mech, 146(1–2), 59–71.
5. Xu H, Liao SJ, Pop I (2007). Series solutions of unsteady three-dimensional MHD flow and heat transfer in the boundary layer over an impulsively stretching plate. Eur J Mech-B/Fluids, 26(1), 15–27.
6. Liu I, Andersson HI (2008). Heat transfer over a bidirectional stretching sheet with variable thermal conditions. Int J Heat Mass Transf, 51(15), 4018–4024.
7. Hayat T, Mustafa M, Hendi AA (2011). Time-dependent three-dimensional flow and mass transfer of elastico-viscous fluid over unsteady stretching sheet. Appl Math Mech, 32(2), 167–178.
8. Hayat T, Awais M, Obaidat S (2012). Three-dimensional flow of a Jeffery fluid over a linearly stretching sheet. Commun Nonlinear Sci Numer Simul, 17(2), 699–707.
9. Liu IC, Wang HH, Peng YF (2013). Flow and heat transfer for three-dimensional flow over an exponentially stretching surface. Chem Eng Commun, 200(2), 253–268.
10. Khan JA, Mustafa M, Hayat T, Farooq MA, Alsaedi A, et al. (2014). On model for three-dimensional flow of nanofluid: An application to solar energy. J Mol Liq, 194, 41–47.
11. Sheikholeslami M, Ganji DD (2014). Numerical investigation for two phase modeling of nanofluid in a rotating system with permeable sheet. J Mol Liq, 194, 13–19.
12. Vajravelu K (2001). Viscous flow over a nonlinearly stretching sheet. Appl Math Comput, 124(3), 281–288.
13. Cortell R (2007). Viscous flow and heat transfer over a nonlinearly stretching sheet. Appl Math Comput, 184(2), 864–873.
14. Bhargava R, Sharma S, Takhar HS, Bég OA, Bhargava P (2007). Numerical solutions for micropolar transport phenomena over a nonlinear stretching sheet. Nonlinear Anal.-Model Control, 12, 45–63.
15. Cortell R (2008). Effects of viscous dissipation and radiation on the thermal boundary layer over a nonlinearly stretching sheet. Phys Lett A, 372(5), 631–636.
16. Hayat T, Abbas Z, Javed T (2008). Mixed convection flow of a micropolar fluid over a non-linearly stretching sheet. Phys Lett A, 372(5), 637–647.
17. Kechil S, Hashim I (2008). Series solution of flow over nonlinearly stretching sheet with chemical reaction and magnetic field. Phys Lett A, 372(13), 2258–2263.
18. Hayat T, Hussain Q, Javed T (2009). The modified decomposition method and Padé approximants for the MHD flow over a non-linear stretching sheet. Nonlinear Anal-Real World Appl, 10(2), 966–973.
19. Ziabakhsh Z, Domairry G, Bararnia H, Babazadeh H (2010). Analytical solution of flow and diffusion of chemically reactive species over a nonlinearly stretching sheet immersed in a porous medium. J Taiwan Inst Chem Eng, 41(1), 22–28.
20. Rana P, Bhargava R (2012). Flow and heat transfer of a nanofluid over a nonlinearly stretching sheet: a numerical study. Commun Nonlinear Sci Numer Simul, 17(1), 212–226.
21. Shahzad A, Ali R, Khan M (2012). On the exact solution for axisymmetric flow and heat transfer over a nonlinear radially stretching sheet. Chinese Phys Lett, 29(8), 084705.
22. Mukhopadhyay S (2013). Analysis of boundary layer flow over a porous nonlinearly stretching sheet with partial slip at the boundary. Alexandria Eng J, 52(4), 563–569.
23. Mukhopadhyay S (2013). Casson fluid flow and heat transfer over a nonlinearly stretching surface. Chinese Phys B, 22(7), 074701.
24. Rashidi MM, Freidoonimehr N, Hosseini A, Bég OA, Hung TK (2014). Homotopy simulation of nanofluid dynamics from a non-linearly stretching isothermal permeable sheet with transpiration. Meccanica, 49(2), 469–482.
25. Rashidi MM, Keimanesh M (2010). Using differential transform method and padé approximant for solving MHD flow in a laminar liquid film from a horizontal stretching surface. Math Prob Eng, 2010 Article ID 491319.
26. Rashidi MM, Pour SM (2010). Analytic approximate solutions for unsteady boundary-layer flow and heat transfer due to a stretching sheet by homotopy analysis method. Nonlinear Anal.-Model Control, 15(1), 83–95.
27. Rashidi MM, Erfani E (2011). The modified differential transform method for investigating nano boundary-layers over stretching surfaces. Int J Numer Methods Heat Fluid Flow, 21(7), 864–883.
28. Sheikholeslami M, Ganji DD (2014). Magnetohydrodynamic flow in a permeable channel filled with nanofluid. Scientia Iranica, 21(1), 203–212.
29. Sheikholeslami M, Gorji-Bandpy M (2014). Free convection of ferrofluid in a cavity heated from below in the presence of an external magnetic field. Powder Technol, 256, 490–498.
30. Sheikholeslami M, Gorji-Bandpy M, Ganji DD, Soleimani S (2014). Thermal management for free convection of nanofluid using two phase model. J Mol Liq, 194, 179–187.
31. Sheikholeslami M, Gorji-Bandpy M, Ganji DD, Rana P, Soleimani S (2014). Magnetohydrodynamic free convection of Al2O3-water nanofluid considering Thermophoresis and Brownian motion effects. Comput Fluids, 94, 147–160.
32. Sheikholeslami M, Gorji-Bandpy M, Ganji DD (2014). Lattice Boltzmann method for MHD natural convection heat transfer using nanofluid. Powder Technol, 254, 82–93.
33. Sheikholeslami M, Ganji DD, Gorji-Bandpy M, Soleimani S (2014). Magnetic field effect on nanofluid flow and heat transfer using KKL model. J Taiwan Inst Chem Eng, 45(3), 795–807.
34. Marinca V, Herişanu N (2008). Application of optimal homotopy asymptotic method for solving nonlinear equations arising in heat transfer. Int Commun Heat Mass, 35(6), 710–715.
35. Niu Z, Wang C (2010). A one-step optimal homotopy analysis method for nonlinear differential equations. Commun Nonlinear Sci Numer Simul, 15(8), 2026–2036.
36. Liao S (2010). An optimal homotopy-analysis approach for strongly nonlinear differential equations. Commun Nonlinear Sci Numer Simul, 15(8), 2003–2016.
37. Abbasbandy S, Shivanian E, Vajravelu K (2011). Mathematical properties of ħ-curve in the frame work of the homotopy analysis method. Commun Nonlinear Sci Numer Simul, 16(11), 4268–4275.

38. Mushtaq A, Mustafa M, Hayat T, Rahi M, Alsaedi A (2013). Exponentially Stretching Sheet in a Powell–Eyring Fluid: Numerical and Series Solutions. Z Naturforsch, 68a(12), 791–798.
39. Mustafa M, Farooq MA, Hayat T, Alsaedi A (2013). Numerical and series solutions for stagnation-point flow of nanofluid over an exponentially stretching sheet. PLoS ONE, 8(5), e61859.
40. Farooq U, Xu H (2014). Free convection nanofluid flow in the stagnation-point region of a three-dimensional body. The Scientific World Journal Article ID 158269.
41. Zhao YL, Liao SJ (2014). Advances in the homotopy analysis method, Chapter 9, World Scientific.